Scaling Law of High Harmonic Generation in the Framework of Photon Channels

Liang Li,[1] Pengfei Lan,[1,*] Lixin He,[1] Xiaosong Zhu,[1,†] Jing Chen,[2,3,5,‡] and Peixiang Lu[1,4,§]

[1]*Wuhan National Laboratory for Optoelectronics and School of Physics,*
Huazhong University of Science and Technology, Wuhan 430074, China
[2]*HEDPS, Center for Applied Physics and Technology, Peking University, Beijing 100084, China*
[3]*Institute of Applied Physics and Computational Mathematics, P. O. Box 8009, Beijing 100088, China*
[4]*Laboratory of Optical Information Technology, Wuhan Institute of Technology, Wuhan 430205, China*
[5]*Collaborative Innovation Center for IFSA (CICIFSA), Shanghai Jiao Tong University, Shanghai 200240, China*

A photon channel perspective on high harmonic generation (HHG) is proposed by quantizing both the driving laser and high harmonics. It is shown that the HHG yield can be expressed as a sum of the contribution of all the photon channels. From this perspective, the contribution of a specific photon channel follows a simple scaling law and the competition between the channels is well interpreted. Our prediction is shown to be in good agreement with the simulations by solving the time-dependent Schrödinger equation. It also can explain well the experimental results of the HHG in the noncollinear two-color field and bicicular laser field.

High harmonic generation (HHG) is a highly nonlinear process in the interaction between the atom (or molecule) and the intense laser field. Attosecond pulses can be generated by coherently synthesizing a series of high harmonics [1–4], which enables us to steer and probe the nuclear and electronic dynamics in an unprecedentedly fast time scale [5–7].

Many theoretical methods have been developed to investigate the HHG. By solving the time-dependent Schrödinger equation (TDSE), one can reproduce the HHG. However, the underlying physics cannot be straightforward revealed since the rich information is encoded in the electronic wave function. Many other approaches such as the Lewenstein model [8], quantum orbits (QO) theory [9–11], quantitatively rescattering (QRS) theory [12–14], and factorization methods [15,16] have been developed. With these theories, the HHG process can be quantitatively described by the electron trajectories (or quantum orbits [9]), and lots of experimental results can be well interpreted, e.g., the cutoff law and the long or short trajectory [17,18].

All the theories mentioned above treat the driving laser and the high harmonics as classical oscillatory electromagnetic waves. Although it has proven quite successful in describing several facets of HHG, it is not convenient to explain the quantized photon properties. However, theories treating the driving laser and the high harmonics as photons are scarce [19–21]. Recently, HHG in the noncollinear two-color laser field [22,23] and nonpure vortex beam [24] are drawing increasing attention in both fundamental studies and applications. To explain the complicated features of high harmonics, the concept of the photon channel was employed. In this case, one can intuitively understand the HHG with photon channels that an atom absorbs and emits

specific numbers of photons based on the selection rules or conservation laws [22–25]. However, the photon channel is only phenomenologically applied. The HHG theory from the photon channel perspective is far from being quantitatively formulated and the underlying physics is still not well understood.

In this Letter, we propose a photon channel perspective on HHG by quantizing the electromagnetic field. From this perspective, the HHG emission yield can be expressed in terms of the photon channels. The contribution of a specific photon channel to HHG follows a simple analytical formula. Then the complicated photonlike features of HHG in the multimode field can be well described, such as the photon channel competition and the scaling law.

We consider the HHG in a two-color field. The laser intensities, frequencies, and wave vectors are denoted as I_1, I_2, ω_1, ω_2 and $\mathbf{k}_1$, $\mathbf{k}_2$, respectively. The frequency and wave vector of the high harmonics are denoted as Ω and $\mathbf{k}'$, respectively. The two-color field and the high harmonics are both quantized. Vacuum polarization and other relativistic effects for the electron are ignored. The Hamiltonian of this atom-radiation system is

$$H = H_0 + H_p + V_L, \tag{1}$$

where $H_0 = \hat{T} + \hat{V}_c$ and $H_p = \omega_1 \hat{N}_1 + \omega_2 \hat{N}_2 + \Omega \hat{N}_\Omega$ are Hamiltonian of the field-free atom and photon, respectively. $\hat{T}$ and $\hat{V}_c$ are the kinetic energy and potential of the electron. $\hat{N}_1 = (a_1^\dagger a_1 + a_1 a_1^\dagger)/2$, $\hat{N}_2 = (a_2^\dagger a_2 + a_2 a_2^\dagger)/2$, $\hat{N}_\Omega = [(a')^\dagger a' + a'(a')^\dagger]/2$ are the photon number operators of the two-color field and the harmonic photon mode, respectively. a and $a^\dagger$ are the annihilation and creation operators. $V_L = -\mathbf{d} \cdot (\mathbf{E}_1 + \mathbf{E}_2 + \mathbf{E}')$ is the electron-photon interaction. The electric fields $\mathbf{E}_m$ ($m = 1$, 2)

and $\mathbf{E}'$ for the driving laser and the generated harmonics can be expressed as $\mathbf{E}_m = ig_m(\hat{\epsilon}_m a_m e^{i\mathbf{k}_m \cdot \mathbf{r}} - \text{c.c.})$ and $\mathbf{E}' = ig'(\hat{\epsilon}' a' e^{i\mathbf{k}' \cdot \mathbf{r}} - \text{c.c.})$. $g_m = (2\omega_m/V)^{1/2}$, $g' = (2\Omega/V')^{1/2}$, where V and V' are the normalization volumes of the driving laser and high harmonics. In the large photon-number limit $g\sqrt{N} \to \sqrt{(I/2)}$ [20]. $\hat{\epsilon}_m = [\hat{\epsilon}_x \cos(\theta_m) + i\hat{\epsilon}_y \sin(\theta_m)]e^{i\eta_m}$ and $\hat{\epsilon}_m^* = [\hat{\epsilon}_x \cos(\theta_m) - i\hat{\epsilon}_y \sin(\theta_m)]e^{i\eta_m}$ are the transverse polarization. θ_m describes the polarization and η_m describes the relative phase. The long-wavelength approximation ($\lambda \gg r_{\text{electron}}$) is adopted here, i.e., $e^{i\mathbf{k}_m \cdot \mathbf{r}} \approx 1$, $e^{i\mathbf{k}' \cdot \mathbf{r}} \approx 1$, and the electric field is independent of r.

To clarify interaction between the atom and the photons, the Hamiltonian is rewritten in the interaction picture

$$H_I(t) = e^{i(H_0 + H_p)t}[-d(\mathbf{E}_1 + \mathbf{E}_2 + \mathbf{E}')]e^{-i(H_0 + H_p)t}$$
$$= -D(t)[\varepsilon_1(t) + \varepsilon_2(t) + \varepsilon'(t)], \tag{2}$$

where $D(t) = e^{iH_0 t} d e^{-iH_0 t}$, $\varepsilon_{1,2}(t) = ig_{1,2}(\hat{\epsilon}_{1,2}a_{1,2}e^{-i\omega_{1,2}t} - \text{c.c.})$, and $\varepsilon' = ig'(\hat{\epsilon}'a'e^{-i\Omega t} - \text{c.c.})$. Then, the transition matrix element between two states $|i\rangle$ and $|f\rangle$ is

$$A(i \to f) = \langle f|e^{-i(H_0 + H_p)t}U_I(t, t_0)|i\rangle, \tag{3}$$

where $U_I(t, t_0)$ is the time-evolution operator in the interaction picture. Using the Dyson equation, U_I can be expressed as [26]

$$U_I(t, t_0) = \sum_{n=0}^{\infty} U_{In}(t, t_0), \tag{4}$$

$$U_{In}(t, t_0) = \left(\frac{1}{i}\right)^n \int_{t_0}^{t} dt_1 ... \int_{t_0}^{t_{n-1}} dt_n H_I(t_1)...H_I(t_n). \tag{5}$$

Substituting Eqs. (2) and (4) into Eq. (3), we have

$$A(i \to f) = \sum_{n=0}^{\infty} \langle f|e^{-i(H_0 + H_p)t}\left(\frac{1}{i}\right)^n \int_{t_0}^{t} dt_1 ...$$
$$\times \int_{t_0}^{t_{n-1}} dt_n H_I(t_1)...H_I(t_n)|i\rangle$$
$$= \sum_{n=0}^{\infty} \sum_{\omega^{t_1}, \omega^{t_2},...,\omega^{t_n}} A_n(\omega^{t_1}, \omega^{t_2}, ..., \omega^{t_n}), \tag{6}$$

$$A_n(\omega^{t_1}, \omega^{t_2}, \omega^{t_3}, ..., \omega^{t_n})$$
$$= \int_{t_0}^{t} dt_1 \int_{t_0}^{t_1} dt_2 ... \int_{t_0}^{t_{n-1}} dt_n$$
$$\times \langle f|e^{-i(H_0 + H_p)t}[-D(t_1)\varepsilon(\omega^{t_1})][-D(t_2)\varepsilon(\omega^{t_2})]...$$
$$\times [-D(t_n)\varepsilon(\omega^{t_n})]|i\rangle, \tag{7}$$

where $\varepsilon(\omega_{1,2}) = \sqrt{(2\omega_{1,2}/V)}\hat{\epsilon}_{1,2}a_{1,2}e^{-i\omega_{1,2}t}$, $\varepsilon(-\omega_{1,2}) = -\sqrt{(2\omega_{1,2}/V)}\hat{\epsilon}_{1,2}^* a_{1,2}^{\dagger} e^{i\omega_{1,2}t}$, $\varepsilon(\Omega) = \sqrt{(2\Omega/V')}\hat{\epsilon}'a'e^{-i\Omega t}$, and $\varepsilon(-\Omega) = -\sqrt{(2\Omega/V')}(\hat{\epsilon}')^*(a')^{\dagger}e^{i\Omega t}$. ω^{t_i} is the frequency of the photon absorbed/emitted at time t_i, i.e., $\omega^{t_i} = \pm\omega_1$, $\pm\omega_2$ or $\pm\Omega$ ("+" denotes absorption and "−" denotes emission).

In our model, the HHG process is described by the transition from the initial state to the final state of the atom via the interaction with the driving photon field. As the strong field approximation in the well-known models [8,15,27,28], the initial and final states are the ground state of the atom. All the transitions between the excited bound states and continuous states and the depletion of the atom are neglected. In detail, the initial and final states in our model are written as $|i\rangle = |\phi_0, N_{1i}, N_{2i}, 0\rangle = \phi_0 \otimes |N_{1i}\rangle \otimes |N_{2i}\rangle \otimes |0\rangle'$ and $|f\rangle = |\phi_0, N_{1f}, N_{2f}, 1\rangle = \phi_0 \otimes |N_{1f}\rangle \otimes |N_{2f}\rangle \otimes |1\rangle'$, which are the eigenstates of the Hamiltonian $H_0 + H_P$ with eigenenergies $E_i = -E_0 + (N_{1i} + \frac{1}{2})\omega_1 + (N_{2i} + \frac{1}{2})\omega_2 + \frac{1}{2}\Omega$ and $E_f = -E_0 + (N_{1f} + \frac{1}{2})\omega_1 + (N_{2f} + \frac{1}{2})\omega_2 + \frac{3}{2}\Omega$, respectively. ϕ_0 is the ground-state wave function of the atomic electron with binding energy E_0. $|N_{1i}\rangle$, $|N_{2i}\rangle$, $|N_{1f}\rangle$, and $|N_{2f}\rangle$ are the Fock states of the laser modes with photon number N_{1i}, N_{2i}, N_{1f}, and N_{2f}. $|0\rangle'$ and $|1\rangle'$ are the Fock states of the high harmonic. According to the energy conservation law, only the terms $A_n(-\Omega; \omega^{t_2}, \omega^{t_3}, ..., \omega^{t_n})$ satisfying $\Omega = \omega^{t_2} + \omega^{t_3} + \cdots + \omega^{t_n}$ contribute to the harmonic Ω. Finally, by using $a|N\rangle = \sqrt{N}|N - 1\rangle$ and $a^{\dagger}|N\rangle = \sqrt{N+1}|N + 1\rangle$, the emission rate of the harmonic Ω can be expressed as (see Sec. A in the Supplemental Material [29])

$$P(\Omega) = |A(i \to f)|^2$$
$$= \left|\sum_{n=0}^{\infty} \sum_{\omega^{t_2},...,\omega^{t_n}} A_n(-\Omega; \omega^{t_2}, ..., \omega^{t_n})\delta(\omega^{t_2} + \cdots + \omega^{t_n} - \Omega)\right|^2$$
$$= \left|\sum_{n=0}^{\infty} \sum_{\omega^{t_2},...,\omega^{t_n}} \sigma_0^{\frac{1}{2}}(-\Omega; \omega^{t_2}, ..., \omega^{t_n})p^{\frac{1}{2}}(|\omega^{t_2}|)...p^{\frac{1}{2}}(|\omega^{t_n}|)\delta(\omega^{t_2} + \cdots + \omega^{t_n} - \Omega)\right|^2. \tag{8}$$

$$\sigma_0^{\frac{1}{2}}(-\Omega; \omega^{t_2}, ..., \omega^{t_n}) = \int_{t_0}^{t} dt_1 ... \int_{t_0}^{t_{n-1}} dt_n \langle\phi_0, N_{1f}, N_{2f}, 1|D(t_1)(\hat{\epsilon}')^*\sqrt{\frac{2\Omega}{V'}}e^{i\Omega t_1}(a')^{\dagger}$$
$$\times (-1)^{n-1}\left(D(t_2)\hat{\epsilon}^{t_2}\sqrt{\frac{I}{2}}e^{-i\omega^{t_2}t_2}\right)...\left(D(t_n)\hat{\epsilon}^{t_n}\sqrt{\frac{I}{2}}e^{-i\omega^{t_n}t_n}\right)|\phi_0, N_{1f}, N_{2f}, 0\rangle, \tag{9}$$

where $\hat{\epsilon}^{t_i} = \hat{\epsilon}_m$ for $\omega^{t_i} = \omega_m$ and $\hat{\epsilon}^{t_i} = -\hat{\epsilon}_m^*$ for $\omega^{t_i} = -\omega_m$ ($m = 1, 2$). $p(\pm\omega_m) = p_m = (I_m/I)$ ($m = 1, 2$) are the ratios of the intensity. $\sigma_0^{\frac{1}{2}}(-\Omega; \omega^{t_2}, \omega^{t_3}, ..., \omega^{t_n})$ describes the ability of emitting a harmonic photon Ω via a quantum path of absorbing a series photons $\omega^{t_n}, \omega^{t_{n-1}}...\, \omega^{t_2}$.

To establish the link between our model and the observable quantity, we introduce the photon channel that is the sum of all the quantum paths involving the same net number (n_1, n_2) of the two-color photons. This photon channel corresponds to the high harmonic $\Omega = n_1\omega_1 + n_2\omega_2$ that is observable in experiment. From the photon channel perspective, the emission rate of the harmonic Ω can be expressed as

$$P(\Omega) = \left|\sum_{n_1, n_2} P^{\frac{1}{2}}(\Omega(n_1, n_2))\delta(n_1\omega_1 + n_2\omega_2 - \Omega)\right|^2$$

$$= \left|\sum_{n_1, n_2} \sigma^{\frac{1}{2}}(n_1, n_2) p_1^{\frac{|n_1|}{2}} p_2^{\frac{|n_2|}{2}} \delta(n_1\omega_1 + n_2\omega_2 - \Omega)\right|^2, \quad (10)$$

where $\sigma^{\frac{1}{2}}(n_1, n_2) = \sum_{[n_1, n_2]} \sigma_0^{\frac{1}{2}}(\Omega; \omega^{t_2}, \omega^{t_3}, ..., \omega^{t_n}) e^{i\varphi_{[n_1, n_2]}}$. $[n_1, n_2]$ indicates an arrangement of net n_1 ω_1 photons and net n_2 ω_2 photons. If different photon channels can be distinguished, i.e., the high harmonic Ω is dominated by only one photon channel, one can rewritten Eq. (10) as $P(\Omega) = \sum_{n_1, n_2} P(\Omega(n_1, n_2))\delta(n_1\omega_1 + n_2\omega_2 - \Omega)$. Note that the net n_m ($m = 1, 2$) photon absorption process may involve absorption of $(n_m + q)$ photons and emission of q photon. Within the strong field approximation [8], we can ignore the influence of the Coulomb potential on the continuous state, and then the sum of all the terms involving extra absorption and emission of the same photons in the summation only give rise to a phase factor (see Sec. B in Ref. [29]). Furthermore, we introduce the permutation symmetry to the parameter σ_0 with the standard method [30] and then σ_0 for different quantum paths in a specific photon channel become equal. Therefore, we have $\sigma(n_1, n_2) = C_{|n_1| + |n_2|}^{|n_1|}\sigma_0(n_1, n_2)$, and $P(\Omega(n_1, n_2)) = \sigma_0(n_1, n_2) C_{|n_1| + |n_2|}^{|n_1|} p_1^{|n_1|} p_2^{|n_2|}$, where $\sigma_0(n_1, n_2)$ is the abbreviation of $\sigma_0(\Omega; \omega^{t_2}, \omega^{t_3}, ..., \omega^{t_n})$. Note that this formula can be separated to two terms: the term σ_0 describes the characteristic structure of the high harmonic spectra and the term $C_{|n_1| + |n_2|}^{|n_1|} p_1^{|n_1|} p_2^{|n_2|}$ corresponds to the weight of the photon channel, which describes the channel competition and power scaling of a specific harmonic (see the discussion below). Interestingly, the second term has similar behavior to the nonlinear optical wave mixing [30]. It indicates that, although HHG is a highly nonperturbative process, the power scaling of its photon channel still follows a perturbative way. A recent experiment has demonstrated this property in the case of $I_2 \ll I_1$ [22]. However, this phenomenon is only explained using a phenomenological scaling of $I_2^{n_2}$ in Ref. [22]. Here we provide a quantitative
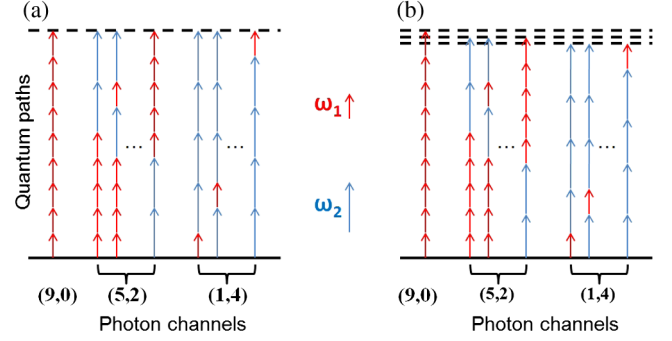

FIG. 1. The sketches of the quantum paths and photon channels of HHG in the two-color field. A photon channel contains many quantum paths as denoted in the brace. (a) The sketch for harmonic $\Omega = 9\omega_1$ with $\omega_1 : \omega_2 = 1 : 2$. In this case, the photon channels $\Omega(9, 0)$, $\Omega(5, 2)$, $\Omega(1, 4)$ are degenerate. (b) The sketch for harmonics $\Omega = 9\omega_1$, $8.8\omega_1$, and $8.6\omega_1$ with $\omega_1 : \omega_2 = 1 : 1.9$.

model for understanding the perturbative property of the photon channel. As shown below, our model will retrieve the same scaling law $I_2^{n_2}$ as in Ref. [22] if $I_2 \ll I_1$. More importantly, our formula still works for stronger I_2, where the $I_2^{n_2}$ scaling law fails. It therefore provides a more complete and comprehensive photon-channel perspective of HHG.

To validate our model, we numerically solve the three dimensional TDSE [29,31] in a two-color field. Incommensurate frequencies $\omega_1 : \omega_2 = 1 : 1.9$ instead of $1 : 2$ are applied to identify the photon channels [25]. As shown in Fig. 1, there are many photon channels, such as $\Omega(9, 0)$, $\Omega(5, 2)$, $\Omega(1, 4)$ and so on, contributing to one harmonic $\Omega = 9\omega_1$ when using a two-color field with frequencies $1 : 2$. By using an incommensurate frequencies $1 : 1.9$, the degenerate channels become distinguishable. The linearly polarized 800 (ω_1) and 421 nm ($\omega_2 = 1.9\omega_1$) fields are adopted in the simulation and the target atom is hydrogen. The relative phase is chosen as $\eta_1 = \eta_2 = 0$. The laser field is turned on linearly over the first 10 optical cycles and is kept constant for another 110 optical cycles. We keep the total intensity $I = I_1 + I_2$ of the two-color field constant (0.2×10^{14} W/cm^2) and vary the ratio $p_2 = I_2/I$.

Figure 2 shows the high harmonic spectra obtained with TDSE for different p_2. The photon channels, e.g., $\Omega(15, 0)$, $\Omega(11, 2)$, and $\Omega(7, 4)$, can be clearly identified. For a small $p_2(= 0.015)$, the channels with small n_2 are dominant, e.g., $\Omega(12, 1)$, $\Omega(15, 0)$, and $\Omega(14, 1)$. This agrees well with our model [see Eq. (10)] that $p_2^{|n_2|}$ rapidly decreases with increasing n_2. One can clearly see from Fig. 2 that the dominant photon channel converts from smaller n_2 to larger n_2 with increasing p_2. For example, the photon channel $\Omega(15, 0)$ converts to $\Omega(11, 2)$, $\Omega(7, 4)$, and so on. One can also see the channel competition, e.g., $\Omega(11, 2)$ and $\Omega(7, 4)$ are comparable for $p_2 = 0.2$. Such a complicated HHG spectrum due to the channel competition can be well predicted and explained with Eq. (10). To evaluate the
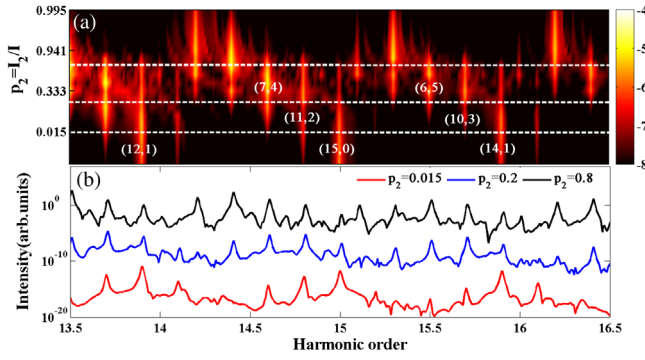
FIG. 2. (a) The HHG spectra for different p_2. Each photon channel for $\Omega = (n_1 + 1.9n_2)\omega_1$ is labeled as (n_1, n_2). The color bar denotes the harmonic yield in logarithmic scale. (b) The HHG spectra for $p_2 = 0.015$, 0.2, and 0.8. The blue and black curves are shifted vertically by multiplying a factor of 10^6 and 10^{12}. All the results are obtained by the three dimensional TDSE.

FIG. 3. High harmonic yield as a function of p_2. The triangles, squares, and circles represent the results with TDSE simulations. The dashed and the dash-dotted curves show the contributions of different photon channels predicted with our model and the solid curves show the sum of them. The laser parameters are the same as Fig. 2. For clarity, the curves for H14.8 and H14.6 are shifted vertically by multiplying a factor of 10^5 and 10^{10}.

channel competition between $\Omega_1(n_1, n_2)$ and $\Omega_2(n'_1, n'_2)$, we introduce the ratio $\gamma(\Omega_1, \Omega_2) = P(\Omega_1(n_1, n_2)) / P(\Omega_2(n'_1, n'_2)) = \gamma_0 C_{|n_1|+|n_2|}^{|n_1|} / C_{|n'_1|+|n'_2|}^{|n'_1|} (1-p_2)^{|n_1|-|n'_1|} p_2^{|n_2|-|n'_2|}$, where $\gamma_0 = \sigma_0(n_1, n_2)/\sigma_0(n'_1, n'_2)$. Here γ_0 can be obtained by solving the equation $\gamma_0 C_{|n_1|+|n_2|}^{|n_1|} / C_{|n'_1|+|n'_2|}^{|n'_1|} (1-p_2)^{|n_1|-|n'_1|} p_2^{|n_2|-|n'_2|} = 1$, where the value of p_2 is determined according to $P(\Omega_1(n_1, n_2)) = P(\Omega_2(n'_1, n'_2))$ in the TDSE simulation. Then, $\gamma(\Omega(15, 0), \Omega(11, 2))$ is calculated to be 10.1 for $p_2 = 0.2$, which predicts that the channel with smaller n_2 $\Omega(15, 0)$ is dominant. For $p_2 = 0.8$, $\gamma(\Omega(7, 4), \Omega(3, 6)) = 0.04$ and the channel with larger n_2 $\Omega(3, 6)$ is dominant.

Next we discuss the scaling law of the harmonic yield for a specific photon channel. It should be noted that the degeneracy of the photon channels cannot be perfectly eliminated even by using the incommensurate frequencies. For example, the same high harmonic Ω can be possibly contributed by both the photon channels $\Omega(n_1, n_2)$ and $\Omega(n_1 - 19, n_2 + 10)$. However, the harmonic Ω is usually dominated by only one photon channel since the ratio $\gamma = \gamma_0 C_{|n_1|+|n_2|}^{|n_1|} / C_{|n_1-19|+|n_2+10|}^{|n_1-19|} (1-p_2)^{|n_1|-|n_1-19|} p_2^{|n_2|-|n_2+10|}$ is a function changing very fast with p_2 (either $\ll 1$ or $\gg 1$ for most values of p_2). Figure 3 shows the high harmonic yield as a function of p_2 on the log-log scale. The triangles, squares, and circles represent the yields of the harmonics $15\omega_1$, $14.8\omega_1$, and $14.6\omega_1$ obtained by numerically solving TDSE, respectively. The dashed and the dash-dotted curves show the harmonic yields contributed by two degenerate photon channels ($\Omega(n_1, n_2)$ and $\Omega(n_1 - 19, n_2 + 10)$) predicted by our model and the solid curves show their sum. We take the yield of harmonic $15\omega_1$ as an example. Our model predicts that the channel $\Omega(15, 0)$ is dominant for $p_2 < 0.3$ and the yield is proportional to $(1-p_2)^{15} p_2^0$. When $p_2 > 0.3$, the dominant channel is converted from
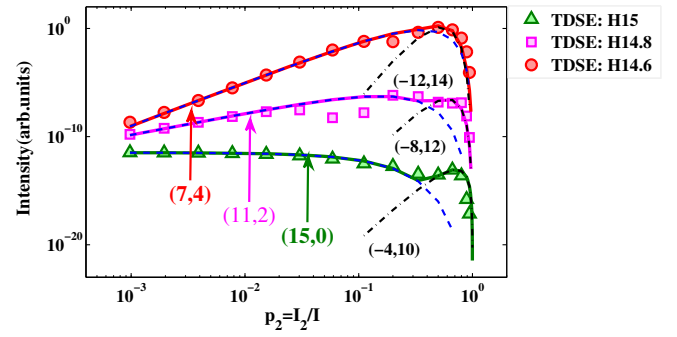
$\Omega(15, 0)$ to $\Omega(-4, 10)$ and the yield is proportional to $(1 - p_2)^4 p_2^{10}$. These predicted scalings are in good agreement with the TDSE simulations. The same agreement is shown in Fig. 3 for harmonics $14.8\omega_1$ and $14.6\omega_1$. In addition, the channel conversion is faster for larger n_1. This can be well explained with the ratio γ. For $\Omega(7, 4)$ and $\Omega(-12, 14)$ with smaller n_1, $\gamma = \gamma_0 C_{11}^4 / C_{26}^{12} (1 - p_2)^{-5} p_2^{-10}$ has a minimum and changes slowly near $\gamma = 1$; i.e., the conversion of the dominant channel is slow. In contrast, for $\Omega(15, 0)$ and $\Omega(-4, 10)$ with larger n_1, $\gamma = \gamma_0 C_{15}^0 / C_{14}^4 (1 - p_2)^{11} p_2^{-10}$ decreases monotonically with p_2 and has a big slope at $\gamma = 1$; i.e., the conversion of the dominant channel is faster. We also performed further simulation with different relative phase and the results show that the scaling law depends insensitively on the relative phase. Moreover, our simulations also confirm the validity of our model in the two-color field with longer wavelength [29].

Our model can be generalized for other forms of laser field rather than only for the collinear two-color field. For example, the emission rate in a noncollinear two-color field can also be obtained as the sum of photon channels by adopting the same procedure as above:

$$P(\Omega, \mathbf{k}') = \sum_{n_1, n_2} P(\Omega(n_1, n_2)) \delta(n_1\omega_1 + n_2\omega_2 - \Omega)$$
$$\times \delta(n_1\mathbf{k}_1 + n_2\mathbf{k}_2 - \mathbf{k}')$$
$$= \sum_{n_1, n_2} \sigma(n_1, n_2) p_1^{|n_1|} p_2^{|n_2|} \delta(n_1\omega_1 + n_2\omega_2 - \Omega)$$
$$\times \delta(n_1\mathbf{k}_1 + n_2\mathbf{k}_2 - \mathbf{k}'). \quad (11)$$

To confirm this, we compare the predictions of our model with the previous work in Ref. [22]. We adopt the same laser intensity as in Ref. [22], where the intensity I_1 is fixed and I_2 is varied. Although the total laser intensity $I = I_1 + I_2$ varies, we still have $p_1 = (I_1/I_1 + I_2)$ and $p_2 = (I_2/I_1 + I_2)$. Assuming that $I_2 \ll I_1$ and the ground
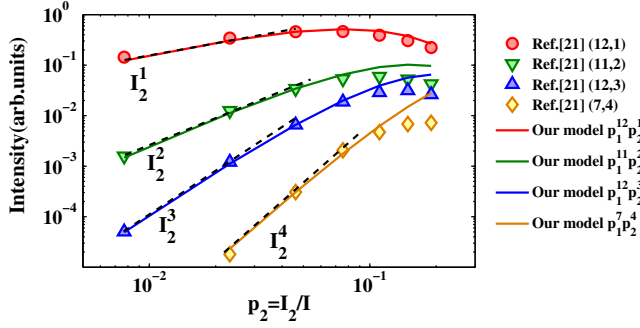
FIG. 4. Comparisons between the HHG yields in the noncollinear two-color field obtained from Ref. [22] (dots) and our model (solid curves). The laser parameters are the same as those in Fig. 3(b) of Ref. [22].

state depletion can be neglected, $\sigma(n_1, n_2)$ is constant and then we have the power scaling as $p_1^{|n_1|} p_2^{|n_2|}$. In Fig. 4, the harmonic yields obtained from Ref. [22] and our model are shown as the dots and solid curves, respectively. When $p_2 < 0.04$, the results in Ref. [22] follow the scalings I_2^1, I_2^2, and I_2^3 for the channels $\Omega(12,1)$, $\Omega(11,2)$, and $\Omega(12,3)$, respectively. However, the harmonic yields in Ref. [22] deviate significantly from the scaling $I_2^{n_2}$ for $p_2 > 0.04$. They become saturated near $p_2 = 0.1$ and even decrease for higher p_2. In contrast, the results obtained with our model agree well with those in Ref. [22] for a larger range. This can be well explained with Eq. (11). In the range of $p_2 < 0.04$, Eq. (11) also gives the scaling $I_2^{n_2}$ since $p_1^{|n_1|} p_2^{|n_2|}$ collapses to $I_2^{|n_2|}$ when $I_2 \ll I_1$. For $p_2 > 0.04$, the contribution of the channel $\Omega(n_1, n_2)$ reaches its maximum at $p_2 = |n_2|/(|n_1| + |n_2|)$ according to Eq. (11). This well explains the saturation effect and the fact that the channel with smaller n_2 saturates earlier. With the intensity I_2 further increased ($p_2 > 0.1$), the total intensity increases obviously. As a result, the factor $\sigma(n_1, n_2)$ cannot be approximated as constant and the harmonic yields obtained from Ref. [22] diverge slowly from those obtained from our model. The above results suggest that the HHG in the noncollinear two-color field can be understood essentially from the photon channel perspective and our model provides a more complete and comprehensive insight of the power scaling law than that in Ref. [22]. It is also worthy noting that the very recent experiment about HHG with bicicular laser pulses has also been explained based on our model [32].

In conclusion, a photon channel perspective of HHG is established by quantizing both the driving laser and high harmonics. Our results indicate that the channel competition and power scaling law follow the similar behavior of the nonlinear optical wave mixing. It well explains the HHG in the two-color field and also explains the experimental results in Ref. [22] beyond the case of $I_2 \ll I_1$. Comparing with the previous models in the wave picture, our work establishes a new and complementary perspective

for understanding the underlying physics of the HHG process in the framework of photon channels. This perspective provides a quantitative approach and useful tool to investigate the quantized photon features in HHG.

[*] pengfeilan@hust.edu.cn
[†] zhuxiaosong@hust.edu.cn
[‡] chen_jing@iapcm.ac.cn
[§] lupeixiang@hust.edu.cn

[1] G. Farkas and C. Toth, Phys. Lett. A **168**, 447 (1992).
[2] I. P. Christov, M. M. Murnane, and H. C. Kapteyn, Phys. Rev. Lett. **78**, 1251 (1997).
[3] P. M. Paul, E. S. Toma, P. Breger, G. Mullot, F. Augé, Ph. Balcou, H. G. Muller, and P. Agostini, Science **292**, 1689 (2001).
[4] M. Hentschel, R. Kienberger, C. Spielmann, G. A. Reider, N. Milosevic, U. Heinzmann, M. Drescher, and F. Krausz, Nature (London) **414**, 509 (2001).
[5] P. B. Corkum and F. Krausz, Nat. Phys. **3**, 381 (2007).
[6] P. Salières, A. Maquet, S. Haessler, J. Caillat, and R. Taïeb, Rep. Prog. Phys. **75**, 062401 (2012); C. Zhai, X. Zhu, P. Lan, F. Wang, L. He, W. Shi, Y. Li, M. Li, Q. Zhang, and P. Lu, Phys. Rev. A **95**, 033420 (2017).
[7] S. Baker, J. S. Robinson, C. A. Haworth, H. Teng, R. A. Smith, C. C. Chirila, M. Lein, J. W. G. Tisch, and J. P. Marangos, Science **312**, 424 (2006); L. He *et al.*, Nat. Commun. **9**, 1108 (2018).
[8] M. Lewenstein, P. Balcou, M. Y. Ivanov, A. L'Huillier, and P. B. Corkum, Phys. Rev. A **49**, 2117 (1994).
[9] W. Becker, F. Grasbon, R. Kopold, D. Milošević, G. Paulus, and H. Walther, Adv. At. Mol. Opt. Phys. **48**, 35 (2002).
[10] P. Salieres *et al.*, Science **292**, 902 (2001).
[11] G. Sansone, C. Vozzi, S. Stagira, and M. Nisoli, Phys. Rev. A **70**, 013411 (2004).
[12] C. D. Lin, A.-T. Le, Z. Chen, T. Morishita, and R. Lucchese, J. Phys. B **43**, 122001 (2010).
[13] T. Morishita, A.-T. Le, Z. Chen, and C. D. Lin, Phys. Rev. Lett. **100**, 013903 (2008).
[14] A.-T. Le, R. R. Lucchese, S. Tonzani, T. Morishita, and C. D. Lin, Phys. Rev. A **80**, 013401 (2009).
[15] M. V. Frolov, A. V. Flegel, N. L. Manakov, and A. F. Starace, Phys. Rev. A **75**, 063407 (2007).
[16] O. Smirnova, Y. Mairesse, S. Patchkovskii, N. Dudovich, D. Villeneuve, P. Corkum, and M. Y. Ivanov, Nature (London) **460**, 972 (2009).
[17] P. B. Corkum, Phys. Rev. Lett. **71**, 1994 (1993).
[18] K. J. Schafer, B. Yang, L. F. DiMauro, and K. C. Kulander, Phys. Rev. Lett. **70**, 1599 (1993).
[19] W. Becker, A. Lohr, M. Kleber, and M. Lewenstein, Phys. Rev. A **56**, 645 (1997).

[20] L. Gao, X. Li, P. Fu, R. R. Freeman, and D.-S. Guo, Phys. Rev. A **61**, 063407 (2000).

[21] B. Wang, L. Gao, X. Li, D.-S. Guo, and P. Fu, Phys. Rev. A **75**, 063419 (2007).

[22] J. B. Bertrand, H. J. Wörner, H.-C. Bandulet, É. Bisson, M. Spanner, J.-C. Kieffer, D. M. Villeneuve, and P. B. Corkum, Phys. Rev. Lett. **106**, 023001 (2011).

[23] D. D. Hickstein *et al.*, Nat. Photonics **9**, 743 (2015).

[24] L. Rego, J. S. Román, A. Picón, L. Plaja, and C. Hernández-García, Phys. Rev. Lett. **117**, 163202 (2016).

[25] A. Fleischer, O. Kfir, T. Diskin, P. Sidorenko, and O. Cohen, Nat. Photonics **8**, 543 (2014).

[26] F. J. Dyson, Phys. Rev **75**, 1736 (1949).

[27] M. V. Frolov, N. L. Manakov, A. A. Silaev, and N. V. Vvedenskii, Phys. Rev. A **81**, 063407 (2010).

[28] M. V. Frolov, N. L. Manakov, T. S. Sarantseva, A. A. Silaev, N. V. Vvedenskii, and A. F. Starace, Phys. Rev. A **93**, 023430 (2016).

[29] See Supplemental Material at http://link.aps.org/supplemental/10.1103/PhysRevLett.120.223203, for details of derivation of our model and additional discussions for different parameters of electric fields.

[30] R. W. Boyd, *Nonlinear Optics* (Elsevier, Singapore, 2010).

[31] M. Protopapas, C. H. Keitel, and P. L. Knight, Rep. Prog. Phys. **60**, 389 (1997), see Chap. 5.

[32] K. M. Dorney *et al.*, Phys. Rev. Lett. **119**, 063201 (2017). The preprint form of our manuscript was cited as Ref. [62] in this reference.